*Microscopy Research and Technique*

WILEY

MICROSCOPY RESEARCH & TECHNIQUE

RESEARCH ARTICLE

# Microscopic Imaging of Alpha Particle Trajectory and Its Application for Radionuclide Distribution Measurement in Cell

Pingping Kong[1] | Changran Geng[1,2] | Xiaowen Tian[1] | Haichao Zhuang[1] | Xiaobin Tang[1,2]

[1]Department of Nuclear Science and Technology, Nanjing University of Aeronautics and Astronautics, Nanjing, China | [2]Key Laboratory of Advanced Nuclear Technology and Radiation Protection, Ministry of Industry and Information Technology, Nanjing, China

**Correspondence:** Changran Geng (gengchr@nuaa.edu.cn)

**Received:** 6 January 2025 | **Revised:** 26 February 2025 | **Accepted:** 8 March 2025

**Review Editor:** Alberto Diaspro

**Funding:** This work is supported by the National Natural Science Foundation of China (Grant No. 12475318, 12261131621) and the National Key Research and Development Program (Grant No. 2022YFE0107800).

**Keywords:** alpha particle | microscope | targeted alpha therapy | trajectory

## ABSTRACT

Imaging and analyzing alpha-particle trajectories are crucial for studying alpha-particle distributions in high-energy physics experiments, such as radioisotope imaging and neutron energy spectrum measurements. This study introduces a novel method that combines an electron-multiplying charge-coupled device (EMCCD) camera, a gadolinium aluminum gallium garnet (GAGG) scintillator film, and a fluorescent microscope to measure the micro-distribution of radionuclides. A reconstruction technique was developed to determine the initial positions of alpha particles based on the pixel gray-value distributions along their trajectories. The effectiveness of this technique was validated through imaging experiments using fixed incident alpha particles. Key imaging parameters, including binning, exposure time, and optical parameters such as magnification, were systematically investigated for their impacts on imaging quality. Results indicated that increasing the binning value improved detection sensitivity but reduced spatial resolution. Shortening exposure times effectively prevented track overlap, aiding trajectory identification, counting, and analysis. Higher magnification of objective lenses enhanced the spatial resolution of the whole system but required greater sample flatness and camera sensitivity. A measurement platform was further developed to explore the cellular distribution of radioactive drugs in targeted alpha therapy. Coupled registration of trajectory and cellular images was achieved using an external Ra-223 source and A549 cells. This trajectory measurement technique is broadly applicable for analyzing the cellular distribution of radioactive drugs in targeted alpha therapy.

## 1 | Introduction

The demand for high-resolution measurement of radioisotope distributions, including the detection of plutonium (Pu) in nuclear facilities and applications in high-energy physics experiments, has significantly increased in recent years (Benabdallah et al. 2024; Goutelard et al. 1998). Alpha-emitting radionuclides have become a prominent focus in radiotherapy research. Due to the limited range of alpha particles, their cellular distribution plays a critical role in determining therapeutic efficacy. In targeted alpha therapy, the heterogeneous distribution of radionuclides affects the biological impact of treatment, adding complexity and uncertainty to radiation dose calculations (Benabdallah et al. 2024). Accurate localization of alpha particles is therefore crucial for optimizing drug development and treatment planning, improving targeting precision, and reducing radiation-induced damage to healthy tissues.

**Summary**

- Incorporating a microscope enables simultaneous capture of ion-track and cellular structure.
- Determining the initial position of the trajectory based on the Bragg curve.
- Optimization of optical and imaging parameters to improve the performance.

Trajectory imaging technology holds significant promise for measuring alpha particle distribution, and numerous efforts have been made to advance alpha-particle trajectory imaging techniques (Chéhadé et al. 2005; Kodaira et al. 2017; Miller et al. 2015; Sohbati et al. 2022). Fluorescent nuclear track detectors (FNTD) and CR-39-based autoradiography offer viable solutions, delivering good spatial resolution for alpha-particle trajectory imaging (Hu et al. 2024; Limam et al. 2023; Russell et al. 2024; Sankowska et al. 2024). However, the complex and time-consuming post-processing required for these methods limits their measurement accuracy and efficiency. This drawback often results in trajectory overlap, complicating subsequent trajectory analysis and reducing overall precision. To address these challenges, Yamamoto et al. 2018 developed a high-resolution alpha-particle imaging system incorporating an electron-multiplying charge-coupled device (EMCCD) camera, a gadolinium aluminum gallium garnet (GAGG) scintillator film, and an AA51. Using this system, they proposed a method to estimate the incident positions of trajectories based on off-focus images (Yamamoto et al. 2020, 2023, 2024a).

In this study, we combined an EMCCD camera with a GAGG scintillator film and a fluorescent microscope to measure the micro-distribution of radionuclides in cells. This approach enables online, high-resolution imaging of alpha-particle trajectories alongside cellular structures. We experimentally investigated the effects of key parameters on trajectory imaging performance, proposing a novel analysis method based on the Bragg curve derived from focused images and optimizing the trajectory measurement technique. The method was preliminarily applied to measure the distribution of alpha-emitting drugs in A549 lung cancer cells using a Ra-223 liquid source.

## 2 | Materials and Methods

### 2.1 | System Prototype and Imaging Processing

Figure 1B illustrates the imaging principle of the system prototype, with the red frame emphasizing the trajectory generation process within the GAGG scintillator. When alpha particles interact with the scintillator, they cause ionization and excitation, depositing all their energy within the material. This process results in the emission of scintillation light along the particles' paths. The image of the scintillation light is then magnified by the microscopic components and captured by a high-sensitivity EMCCD camera, producing a trajectory image. Figure 1A shows the imaging system prototype, which consists of a fluorescence microscope (NM900, Nexcope), a GAGG scintillator, and an EMCCD camera (iXon Ultra 888, Andor). To ensure accurate imaging, the entire system was shielded from ambient light.

In this system, the scintillator is crucial in determining imaging performance (Murata et al. 2022; Zhu et al. 2020). GAGG was selected for alpha-particle detection due to its high light output, excellent transparency, efficient detection capabilities, and durability. To minimize focusing challenges and effectively capture the entire alpha-particle trajectory, a thin scintillator (dimensions: 10 mm × 10 mm × 0.03 mm) was employed. For image acquisition, we utilized a high-sensitivity EMCCD camera, a single-photon detector with an image resolution of 1024 × 1024 pixels and a pixel size of 13 μm × 13 μm. The camera operates in kinetic acquisition mode with a readout rate of 10 MHz and an electron multiplier gain of 50. The system also incorporates three objective lenses, enabling image capture at varying magnifications. Table 1 outlines the properties of these lenses, highlighting their potential impact on the system's imaging performance.

The images captured by the system were processed by ImageJ software (Fiji 2.14.0) (Schindelin et al. 2015). The trajectory length was calculated by multiplying the number of pixels by the pixel size. To determine the system's spatial resolution, we analyzed the distribution curve of pixel intensity along the short axis of the trajectory. The full width at half maximum (FWHM) was then calculated using the Gaussian fitting algorithm in Origin 2018 (Moberly et al. 2018). The signal-to-noise

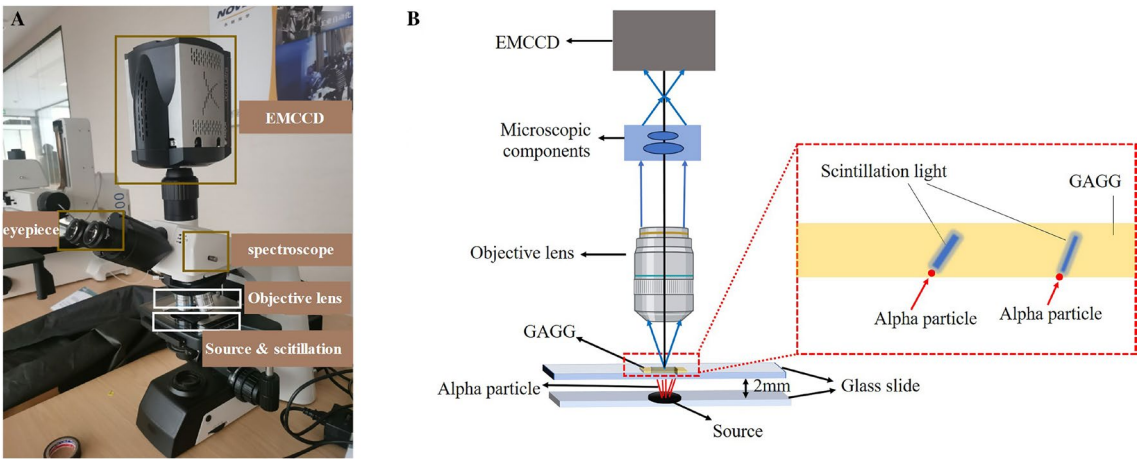


**FIGURE 1** | (A) Imaging system; and (B) imaging principle of the entire system.

ratio (SNR) of the image was assessed by comparing the average gray value of the pixel along the trajectory with the standard deviation (SD) of the background, excluding the trajectory.

## 2.2 | Reconstruction Technique for Estimating the Initial Position of Alpha Particles

Determining the initial position of the particle trajectory can offer more accurate information about the alpha particle's location. Yamamoto et al. suggested using the off-focus image of the trajectory to determine the incident direction, thereby deriving the initial position (Yamamoto et al. 2024b). In this study, we focus primarily on the Bragg curves of alpha particles. For alpha particles with energies exceeding 0.9 MeV, the deposited energy initially increases slowly before rapidly decreasing, as reflected by the pixel intensity distribution along the longitudinal axis of the trajectory. The trajectory length of an alpha particle with energy of 0.9 MeV in GAGG is approximately 2 μm, corresponding to four pixels in a trajectory image obtained with a 100× objective lens. Therefore, for captured trajectory images of alpha particles, if the trajectory length is $<4$ pixels, the midpoint of the trajectory is considered the initial position, as this results in a shorter trajectory and smaller error in determining the initial position. However, when the trajectory length exceeds four pixels, the initial position is determined based on the Bragg peak characteristics of the particle.

**TABLE 1** | Optical properties of the objective lens.

| Objective lens type | Magnification | Numerical aperture | Depth of field (μm) |
|---|---|---|---|
| 1 | 20× | 0.45 | 2.62 |
| 2 | 50× | 0.8 | 0.82 |
| 3 | 100× | 0.9 | 0.65 |

Figure 2 illustrates the methodology for determining the initial position along an alpha-particle trajectory when the length exceeds four pixels. The process begins with the acquisition of the alpha-particle trajectory image, which is then binarized to distinguish the trajectory from the background. Skeletonization is applied to the binarized image, reducing the trajectory to a one-pixel-wide representation, allowing for precise analysis. The two endpoints of the skeletonized trajectory, labeled as A and B, are identified using an endpoint detection algorithm. The integral gray values along the short axis of the trajectory at the two endpoints are denoted as $I_A$ and $I_B$, respectively. The distribution curve of the integral gray values between points A and B is calculated, and the point with the maximum integral gray value is identified as the Bragg peak, denoted as P, with an integral gray value $I_P$. The distance between point A and the Bragg peak is $D_{\overline{AP}}$, and the distance between point B and the Bragg peak is $D_{\overline{BP}}$. The absolute slopes between points A, B and the Bragg peak are calculated as:

$$K_A = \frac{|I_A - I_P|}{D_{\overline{AP}}} \tag{1}$$

$$K_B = \frac{|I_B - I_P|}{D_{\overline{BP}}} \tag{2}$$

respectively. The point with the smaller absolute slope is identified as the initial position of the alpha particle.

## 2.3 | Experimental Setup for Alpha-Particle Distribution Mapping

To verify the feasibility of the proposed trajectory imaging method for measuring radiopharmaceutical cellular distribution in Targeted Alpha Therapy (TAT), an experiment was conducted to measure alpha-particle distribution using a Ra-223 source and A549 cells. Figure 3 illustrates the complete experimental procedure for alpha-particle distribution mapping, which can be divided into five main steps:

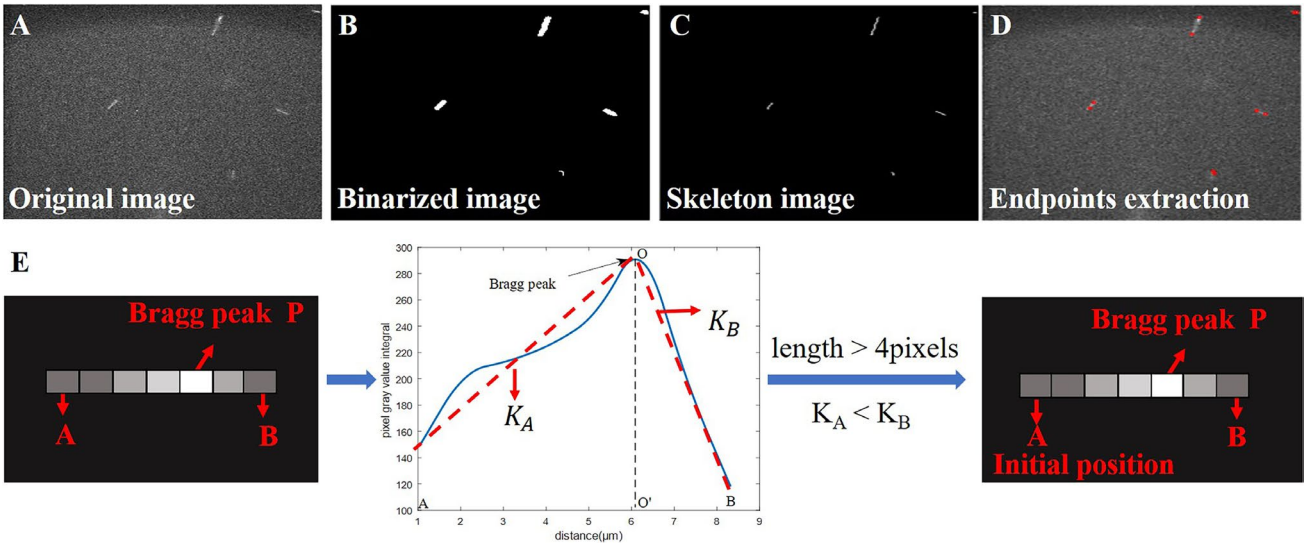


**FIGURE 2** | Extraction of endpoints and determination of the initial position for the particle based on trajectories in images.

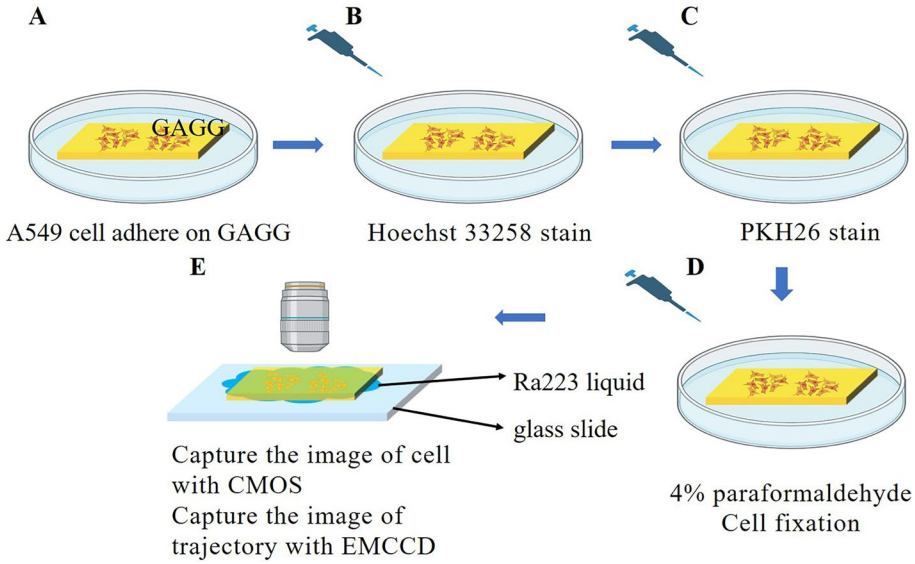


**FIGURE 3** | Schematic of the experimental procedure for alpha-particle distribution mapping.

A. A sterilized GAGG slide is placed in a Petri dish, allowing the A549 lung cells to adhere to its surface.

B. Hoechst 33258 is dropped on the surface of the GAGG slide for 15 min to stain the nuclei of the A549 cells.

C. PKH26 is dropped onto the surface of the GAGG slide for 15 min to stain the cytoplasm of the A549 cells.

D. After staining, the GAGG slide, now covered with adherent cells, is immersed in a 4% paraformaldehyde solution for 20 min to preserve cell morphology and structure.

E. A 10 μL drop of Ra-223 (3 kBq) liquid source is placed on a glass slide, and the cell side of the GAGG is positioned near the Ra-223 source. Images of the cytoplasm and nucleus of the A549 cells are captured using a 20× objective on the microscope with a CMOS camera (NDC 20, Nxcope), while the trajectory of alpha particles penetrating the cells is captured using the developed imaging system with an EMCCD camera.

## 3 | Results

### 3.1 | Influence of Camera Imaging Parameters on Imaging Performance

Imaging experiments of alpha particles from Am-241 were performed under three different binning settings (1×1, 2×2, and 4×4) to investigate the impact of camera imaging parameters on the system's imaging performance. Figure 1B shows the overall layout of the scintillator, radioactive source, and objective lens in the system. The energy of the alpha particles from Am-241 was 4.5 MeV, and the exposure time of the EMCCD camera was set to 2.5 s. Figure 4A–C illustrate the captured images of alpha-particle trajectories under the different binning settings using a 100× objective lens. The SNR and spatial resolutions of the images for the three binning configurations are indicated in these figures. Several line-shaped signals corresponding to the trajectories of the alpha particles are visible. From the images marked with red arrows, discerning the trajectories at the 1×1 binning setting proved challenging. As the binning value increased, the trajectories became more discernible, with a slight increase in the width of the trajectories. Figure 4D–F display the pixel intensity distribution curves along the longitudinal axis of a single trajectory for each binning setting. A larger binning setting reduces the number of pixels per trajectory, which decreases the granularity of intensity variations but results in higher peak pixel intensities.

To investigate the effect of exposure time on the imaging of alpha-particle trajectories, imaging experiments were conducted with varying exposure times with the EMCCD camera under a 100× objective lens. The binning mode of the EMCCD camera was set to 4×4. Alpha-particle imaging was performed with exposure times of 0.1, 1, and 2 s. The resulting images of alpha-particle trajectories from the Am-241 radioactive source are shown in Figure 4G–I. As the exposure time increased, the number of visible trajectories in the images also increased. However, this increase was accompanied by a higher occurrence of trajectory overlaps. Figure 4I highlights one such overlap, where two trajectories overlapping are clearly visible within the red frame. These overlaps complicate the identification and analysis of individual trajectories, potentially reducing the accuracy and precision of the trajectory analysis.

### 3.2 | Influence of Optical Parameters on Imaging Performance

To explore the influence of optical parameters on alpha-particle trajectory imaging, experiments were conducted using objective lenses with magnifications of 20×, 50×, and 100×. The exposure time of the EMCCD camera was set to 1 s, and the binning mode was set to 4×4. The trajectory images captured under different objective magnifications are presented in Figure 5A–C. As the magnification increased, the alpha-particle trajectories

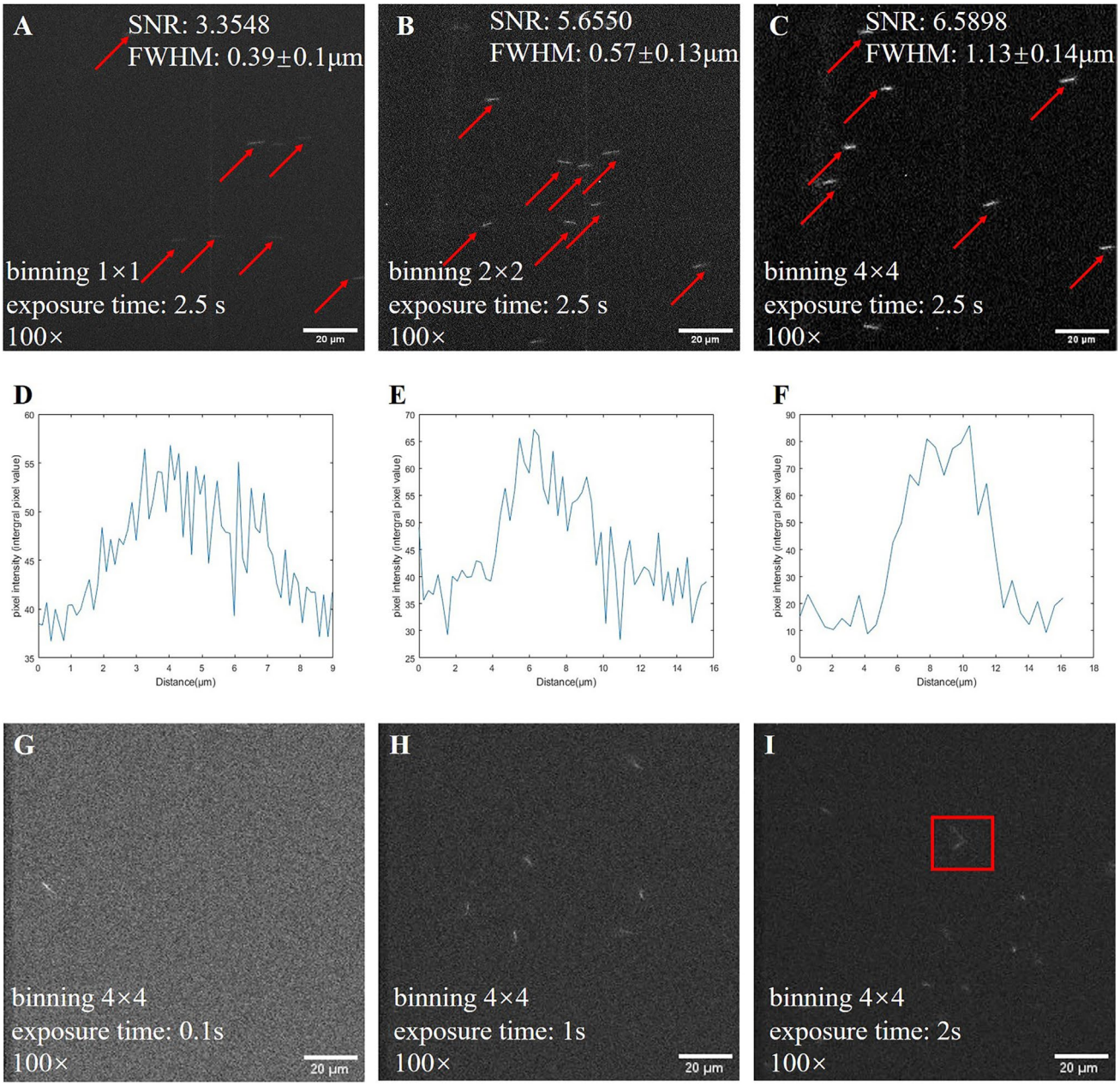


**FIGURE 4** | (A)–(C) Alpha-particle trajectory images (100×, exposure time 2.5 s) captured by the system from Am-241 in different binning modes; and (D)–(F) the corresponding pixel intensity distribution curves along the longitudinal axis of the trajectory in each mode; (G)–(I) Alpha-particle trajectory images (100×, binning 4 × 4) captured by the system from Am-241 with different exposure times.

transitioned from dot-like shapes to short-line and long-line shapes. This change corresponded to an increase in the number of pixels per trajectory, allowing for more detailed trajectory information. However, higher magnification also resulted in a reduced field of view, meaning fewer trajectories were captured in a single frame.

For the images captured with different objective magnifications, the pixel intensity distribution curve along the lateral direction of a single trajectory is shown in Figure 5D–F. Gaussian fitting was applied to the lateral profiles to calculate the full width at half maximum (FWHM), which was used to quantify the spatial resolution. It was observed that the width of the lateral intensity curves decreased with higher magnifications, indicating enhanced spatial resolution. Table 2 summarizes the overall spatial resolutions of the system under the different objective lenses. As the magnification increased, the spatial resolution of the system improved, providing more precise imaging of alpha-particle trajectories.

### 3.3 | Validation of the Method for Estimating the Initial Position of the Particle

In this study, alpha particles interact with the GAGG scintillator, generating trajectories that represent the path of the alpha particles within the material. To precisely localize the initial position of the alpha particles, we propose a reconstruction method based on trajectory information. To assess the accuracy of the

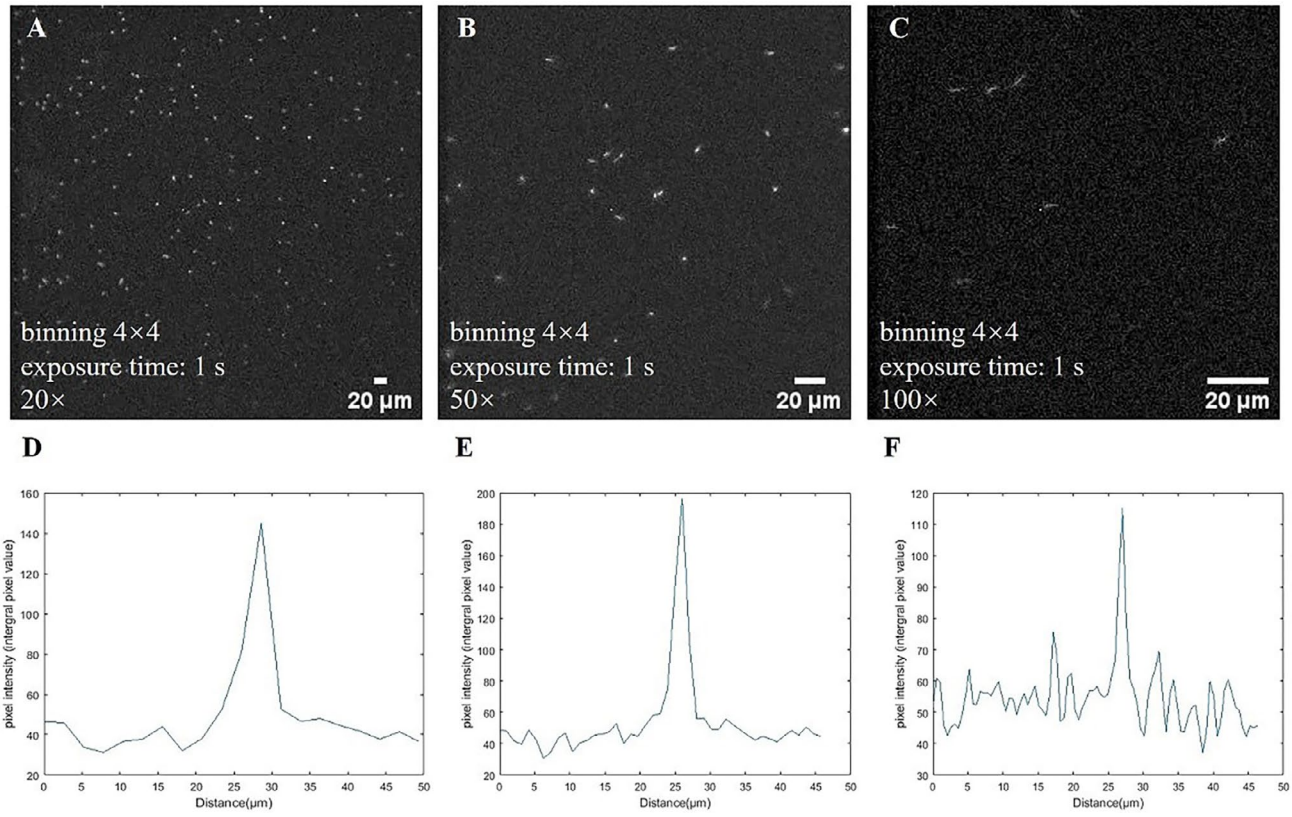


**FIGURE 5** | (A) 20×, binning 4×4, exposure time 1 s, trajectory image captured by the system from Am-241; (B) 50×, binning 4×4, exposure time 1 s, trajectory image captured by the system from Am-241; (C) 100×, binning 4×4, exposure time 1 s, trajectory image captured by the system from Am-241; (D) pixel intensity distribution curve along the lateral axis of a single trajectory from (A); (E) pixel intensity distribution curve along the lateral axis of a single trajectory from (B); (F) pixel intensity distribution curve along the lateral axis of a single trajectory from (C).

**TABLE 2** | The overall spatial resolution of the system under different objective lenses.

| | 20× (NA = 0.45) | 50× (NA = 0.8) | 100× (NA = 0.9) |
|---|---|---|---|
| FWHM (spatial resolution) μm | 3.40 ± 0.3 | 1.95 ± 0.1 | 1.13 ± 0.1 |

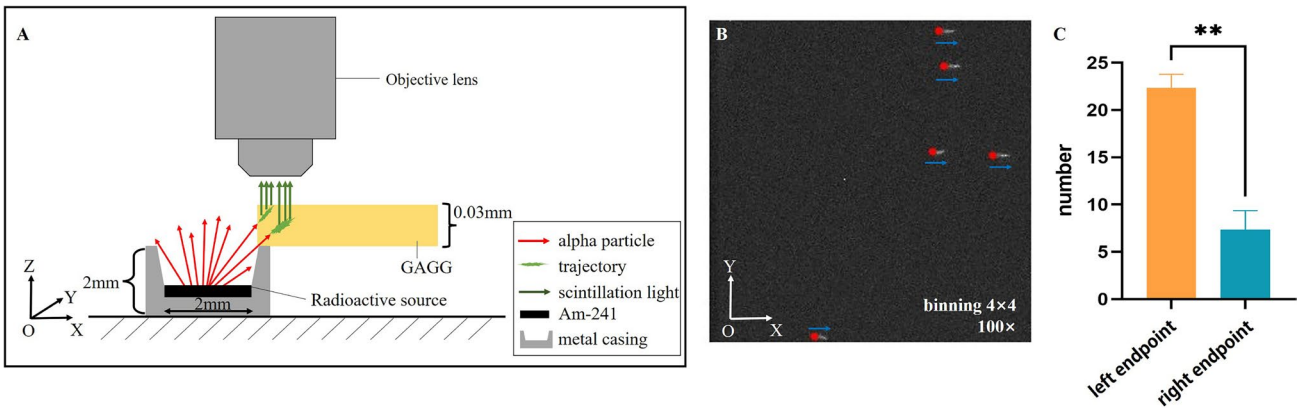


**FIGURE 6** | (A) The relative positions of the Am-241 source, GAGG scintillator, and objective lens unit in the XOZ plane and the formation process of the alpha-particle trajectory with fixed incident direction; (B) Visualization of the initial position determination for trajectory images, with red dots indicating the identified initial positions of the trajectories and blue arrow indicating the real incident direction of alpha particles; (C) Statistical analysis of the accuracy of initial position determinations based on trajectory images (Data are means + SD, $^{**}p < 0.01$).

proposed method, an experiment was proposed by imaging alpha particles with a fixed incident direction. Figure 6A shows the experimental setup, including the relative positioning of the radioactive source, glass slide, GAGG, and the microscopic objective lens. This figure also shows the interaction of alpha particles emitted from the Am-241 source with the GAGG. Since

the alpha particles produced by the Am-241 source are anisotropic, only particles incident along the positive *X*-axis will interact with the GAGG. Theoretically, this setup ensured that the alpha particles entering the scintillator were directed along the positive *X*-axis. In other words, the alpha particles originated from the left endpoint of the trajectory in this experiment.

Under this configuration, a total of 50 images of alpha-particle trajectories were captured with an exposure time of 0.5 s. The experiment was repeated four times for consistency and reproducibility. Then, the proposed reconstruction method was applied to identify the initial positions of the trajectories in all captured images. The results of initial-position identification were divided into two groups: "left endpoint," indicating the initial positions of alpha particles identified as the left endpoints of the trajectory, and "right endpoint," which corresponded to the initial positions of alpha particles identified as the right endpoints of the trajectory. To statistically evaluate the results, a two-sample *t*-test was performed to compare the mean number of trajectories between the two groups. The statistical analysis, shown in Figure 6C, revealed that the proposed method achieved an accuracy of 77% in determining the initial positions of the alpha-particle trajectories.

### 3.4 | Distribution Map of Alpha Particle Penetrating A549 Cells

To evaluate the feasibility of the proposed trajectory imaging method for measuring the cellular distribution of radiopharmaceuticals in targeted alpha therapy (TAT), an experiment was conducted using a Ra-223 source and A549 lung cancer cells. Figure 3 provides an overview of the alpha-particle distribution mapping procedure. In this experiment, A549 cells were cultured on the surface of a GAGG scintillator, with a Ra-223 solution placed beneath the scintillator. Several bubble regions were created within the field of view (FOV) to simulate areas with low-activity radioactive sources, as shown in Figure 7A–G. With the binning set to 1×1, the system's single pixel size is 0.65 μm × 0.65 μm, resulting in an imaging field of view of approximately 665 μm × 665 μm. Given that the A549 cells used in this study have an average diameter of about 12.5 μm, approximately 100 cells were captured in this fixed field of view.

Bright-field fluorescence imaging was used with a CMOS camera to capture the structural details of the cells, while the trajectory images of the alpha particles were recorded using an EMCCD camera. The cell structure images captured by the CMOS camera were fused and registered, creating a composite cellular structure image (Figure 7C). Figure 7E displays the region of interest (ROI) images of the trajectories after threshold segmentation. These two sets of images were then registered and merged to visualize the distribution of the alpha-particle trajectories, using the bubble regions as reference points in the composite cell and trajectory ROI maps.

The white, line-like signals in the images represent the alpha-particle trajectories, which show that the alpha particles emitted from the Ra-223 source can penetrate the A549 cell layer and be detected by the imaging system. Image registration was accomplished using the BigWrap plug-in ImageJ software (Bogovic et al. 2016), and Figure 7G demonstrates the alignment of reference points, confirming a well-matched positional relationship between the cell structure and trajectory images. This alignment allowed for the observation of the relative positioning of alpha particles in relation to the cytoplasm and nucleus of A549 cells, enabling analysis of the cellular distribution of alpha-emitting drugs.

Figure 7H illustrates the statistical results for the alpha-particle trajectories per unit area in low- and high-activity regions. A two-sample *t*-test was performed to compare the mean number of trajectories between the two groups, and the results revealed a significant difference, with the number of trajectories per unit area in the low-activity region being much lower than in the high-activity region. These findings indicate that the proposed imaging method is well-suited for accurately measuring the distribution of alpha-emitting drugs in targeted alpha therapy.

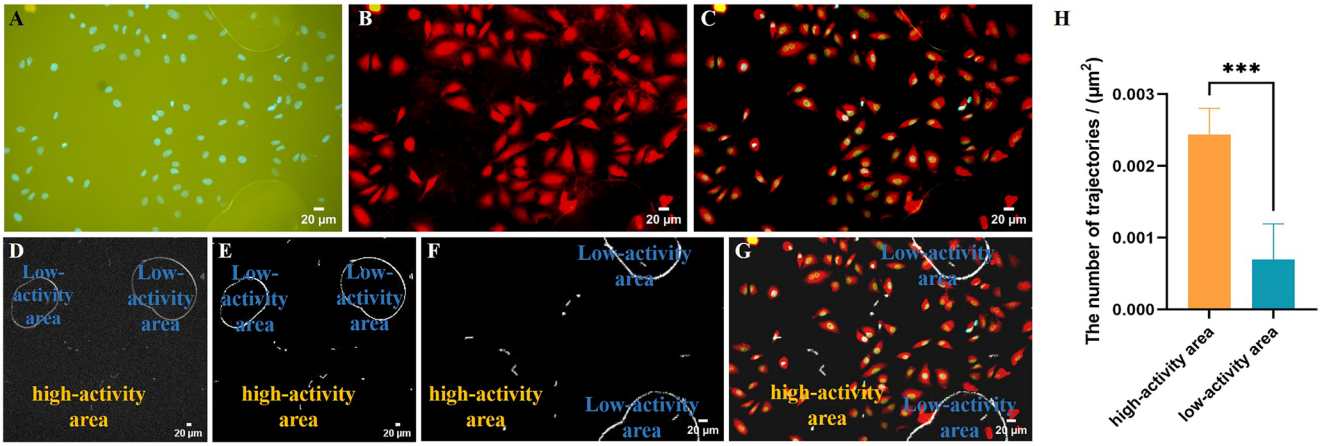


**FIGURE 7** | (A) Fluorescence image of the A549 cell nucleus; (B) Fluorescence image of the A549 cell cytoplasm; (C) Composite cell image of A549 cells. (D) Image of alpha particle trajectory penetrating the A549 cell layer; (E) ROI image of the particle trajectory after threshold segmentation; (F) Bigwrap-transformed image of the alpha-particle trajectory; (G) Distribution map of the alpha particle trajectory penetrating the cell; (H)The statistics of trajectories in the bubble area and outside the bubble area in trajectory images (Data are means + SD, ***$p < 0.001$).

## 4 | Discussion

Trajectory imaging technology holds significant potential for measuring alpha-particle distribution, and this study introduces a novel method using an electron-multiplying charge-coupled device (EMCCD) camera, a GAGG scintillator, and a fluorescence microscope. This approach facilitates online, high-resolution imaging of alpha-particle trajectories. Unlike prior systems that relied on magnifying units, the microscope-based design of this system offers the flexibility of interchangeable objective lenses, enhancing its versatility. The system captures both microscopic distribution images in bright-field and fluorescence modes and alpha-particle trajectory images in light-shielded environments. Additionally, it supports multi-scale alpha-particle measurements, increasing its application flexibility.

The study examined the influence of camera imaging parameters and optical settings on the system's performance. The impact of binning on imaging quality was evaluated through experiments with alpha particles from Am-241 under three binning configurations ($1\times1$, $2\times2$, and $4\times4$). The results showed that increasing binning significantly enhanced the system's sensitivity, improving the recognition of alpha-particle trajectories, particularly in conditions with low particle flux. Additionally, the effect of exposure time on imaging performance was assessed. Imaging experiments with alpha-particle trajectories from Am-241 were conducted at various exposure times. It was observed that longer exposure times led to more frequent trajectory overlaps, which complicate trajectory counting and analysis. This finding suggests that increasing exposure times will increase the likelihood of overlapping trajectories, making accurate analysis more challenging. Unlike traditional autoradiography methods, such as CR-39 and FNTD, the proposed method addresses this issue by reducing the exposure time, effectively minimizing trajectory overlap and thereby improving the accuracy of trajectory analysis. Furthermore, the study assessed the impact of different objective lenses on imaging performance. The choice of objective lens greatly affects spatial resolution. High magnification lenses, such as the 100× objective, offered superior spatial resolution ($0.39\pm0.1\,\mu m$). However, higher magnification also comes with a smaller depth of field, requiring a thinner scintillator and flatter samples to maintain focus.

The study also proposed a novel method for determining the incident positions of alpha particles, enhancing positional resolution. This method accurately determined the initial positions of alpha-particle trajectories from Am-241 with an accuracy of 77%. Unlike prior approaches, this method proposed by Yamamoto et al. (2020) uses focused images to estimate the positions of particles. Analysis showed that the method was more reliable on trajectory images with clear Bragg peaks, with errors occurring more frequently in images with less distinct Bragg peaks. Further improvements in imaging resolution will enable more accurate capture of pixel grayscale variations along the alpha-particle trajectory, enhancing the accuracy of the initial position determination.

In experiments involving A549 lung cancer cells, the distribution of alpha particles penetrating the cancer cells was mapped by registering trajectory and cellular structure images. The analysis revealed a higher density of trajectories in the high-activity regions, correlating with the distribution of the Ra-223 source. This method offers new insights into the cellular distribution of alpha-emitting drugs.

While the results are promising, several aspects require further development. The investigation into factors that influence imaging performance, such as the readout rate of the EMCCD and the properties of the scintillator, is ongoing. Additionally, research on the practical application of this method for assessing the distribution of radioactive drugs in targeted alpha therapy remains limited. Future work will focus on drug incubation experiments to further explore this potential application.

Although the developed technique provides high-resolution online measurements for radioactive drugs, the statistical robustness of the system for cell analysis may be insufficient at this stage. The limited density of cells adhering to the surface of GAGG and the constrained imaging area are primary factors affecting the system's statistical capabilities. To address these limitations, we propose two key strategies: enhancing cell density on the surface of GAGG and expanding the imaging area. First, optimizing cell culture conditions to promote better cell adhesion should be considered, or applying a cell suspension directly onto the surface of GAGG could increase the density of cells within the field of view. Second, expanding the imaging area can be achieved through scanning imaging. This involves adjusting the horizontal position (XY axis) of the microscope stage to sequentially capture images of both radionuclides and cells in different fields of view, while ensuring consistent irradiation times to maintain data consistency. Additionally, integrating the wide-field microscopic device, such as the RUSH3D system, which offers high optical resolution and a wide field of view ($2.6\,mm\times2.0\,mm$ with a lateral resolution of 400 nm), could significantly expand the field of view while maintaining precise measurements (Fan et al. 2019).

## 5 | Conclusion

In summary, this study introduced a novel method for measuring the micro-distribution of radionuclides in cells using an EMCCD camera, a GAGG scintillator film, and an optical microscope. Unlike previous systems that relied on the AA51 magnifying unit, the proposed microscope-based design offers interchangeable objective lenses, enhancing versatility. The influence of imaging and optical parameters of both the microscope and the EMCCD camera on imaging performance was thoroughly investigated. In comparison to autoradiography techniques, such as CR-39 and FNTD, the proposed method effectively reduces trajectory overlap by lowering the exposure time, thereby improving the accuracy of trajectory analysis. A new approach for estimating the initial positions of alpha particles from focused trajectory images was developed, achieving an accuracy of 77%. The study also applied this technique to investigate the radionuclide distribution using A549 cells and a Ra-223 source. The distribution of the alpha-particle trajectories closely matched that of the radionuclide,

with distinct measurements in low-activity and high-activity regions. These results confirm that the proposed technique is suitable for examining the distribution of alpha-emitting drugs within cells.

### Author Contributions

**Pingping Kong:** conceptualization; formal analysis; methodology; software; writing – original draft. **Changran Geng:** conceptualization; project administration; methodology; supervision; data curation; formal analysis; writing – review and editing. **Xiaowen Tian:** formal analysis; software. **Haichao Zhuang:** formal analysis; software. **Xiaobin Tang:** project administration; writing – review and editing.


### Acknowledgments

The authors are grateful to NOVEL for the provision of equipment and technical support. Special thanks to Manager Tan for his assistance with optical techniques. We would like to thank Dr. Feng Tian for helping with that drug distribution experiment.


### Ethics Statement

The authors have nothing to report.

### Consent

The authors have nothing to report.

### Conflicts of Interest

The authors declare no conflicts of interest.

### Data Availability Statement

The data that support the findings of this study are available from the corresponding authors upon reasonable request.

### References


Benabdallah, N., P. Lu, D. S. Abou, et al. 2024. "Beyond Average: α-Particle Distribution and Dose Heterogeneity in Bone Metastatic Prostate Cancer." *Journal of Nuclear Medicine: Official Publication, Society of Nuclear Medicine* 65, no. 2: 245–251. https://doi.org/10.2967/jnumed.123.266571.

Bogovic, J. A., P. Hanslovsky, A. Wong, and S. Saalfeld. 2016. "Robust Registration of Calcium Images by Learned Contrast Synthesis." In *2016 IEEE 13th International Symposium on Biomedical Imaging (ISBI)*, 1123–1126. IEEE. https://doi.org/10.1109/ISBI.2016.7493463.

Chéhadé, F., C. de Labriolle-Vaylet, N. Moins, et al. 2005. "Secondary Ion Mass Spectrometry as a Tool for Investigating Radiopharmaceutical Distribution at the Cellular Level: The Example of I-BZA and 14C-I-BZA." *Journal of Nuclear Medicine* 46, no. 10: 1701–1706.

Fan, J., J. Suo, J. Wu, et al. 2019. "Video-Rate Imaging of Biological Dynamics at Centimetre Scale and Micrometre Resolution." *Nature Photonics* 13, no. 11: 809–816. https://doi.org/10.1038/s41566-019-0474-7.

Goutelard, F., M. Morello, and D. Calmet. 1998. "Alpha-Spectrometry Measurement of am and cm at Trace Levels in Environmental Samples Using Extraction Chromatography." *Journal of Alloys and Compounds* 271: 25–30. https://doi.org/10.1016/S0925-8388(98)00017-6.

Hu, J., T. Kusumoto, M. Janik, and S. Kodaira. 2024. "Alpha Particle Spectrometry in Fluorescent Nuclear Track Detectors With an Automatic 3D Track Reanalysis Algorithm." *Radiation Measurements* 170: 107051. https://doi.org/10.1016/j.radmeas.2023.107051.

Kodaira, S., H. K. Li, T. Konishi, H. Kitamura, M. Kurano, and S. Hasegawa. 2017. "Validating α-Particle Emission From 211At-Labeled Antibodies in Single Cells for Cancer Radioimmunotherapy Using CR-39 Plastic Nuclear Track Detectors." *PLoS One* 12, no. 6: e0178472. https://doi.org/10.1371/journal.pone.0178472.

Limam, S., A. Guittoum, Z. Lounis-Mokrani, M. Hemous, and N. Bendjedda. 2023. "Studying Alpha Irradiated CR39 Using Positron Annihilation Spectroscopy." *Acta Physica Polonica, A* 144, no. 3: 163–172. https://doi.org/10.12693/APhysPolA.144.163.

Miller, B. W., S. H. Frost, S. L. Frayo, et al. 2015. "Quantitative Single-Particle Digital Autoradiography With α-Particle Emitters for Targeted Radionuclide Therapy Using the iQID Camera." *Medical Physics* 42, no. 7: 4094–4105. https://doi.org/10.1118/1.4921997.

Moberly, J. G., M. T. Bernards, and K. V. Waynant. 2018. "Key Features and Updates for Origin 2018." *Journal of Cheminformatics* 10: 1–2. https://doi.org/10.1186/s13321-018-0259-x.

Murata, I., S. Kusaka, K. Minami, et al. 2022. "Design of SPECT for BNCT to Measure Local Boron Dose With GAGG Scintillator." *Applied Radiation and Isotopes* 181: 110056. https://doi.org/10.1016/j.apradiso.2021.110056.

Russell, L., T. M. Johnson, Y. Lawrence, et al. 2024. "Quantifying the Effects of Neutron Fluence on Proton Signal Retention in CR-39." *Review of Scientific Instruments* 95, no. 10: 103505. https://doi.org/10.1063/5.0219479.

Sankowska, M., P. Bilski, M. Kłosowski, A. Kilian, W. Gieszczyk, and B. Marczewska. 2024. "Isotopically Enriched Lithium Fluoride Crystals for Detection of Neutrons With the Fluorescent Track Technique." *Materials* 17, no. 20: 5029. https://doi.org/10.3390/ma17205029.

Schindelin, J., C. T. Rueden, M. C. Hiner, and K. W. Eliceiri. 2015. "The ImageJ Ecosystem: An Open Platform for Biomedical Image Analysis." *Molecular Reproduction and Development* 82, no. 7–8: 518–529. https://doi.org/10.1002/mrd.22489.

Sohbati, R., M. Kook, M. Jain, K. J. Thomsen, and A. Murrey. 2022. "Development of a Wide-Field High-Resolution Ccd Camera-Based Alpha Imaging System." https://doi.org/10.2139/ssrn.4068383.

Yamamoto, S., Y. Hirano, K. Kamada, and A. Yoshikawa. 2020. "Development of an Ultrahigh-Resolution Radiation Real-Time Imaging System to Observe Trajectory of Alpha Particles in a Scintillator." *Radiation Measurements* 134: 106368. https://doi.org/10.1016/j.radmeas.2020.106368.

Yamamoto, S., K. Kamada, and A. Yoshikawa. 2018. "Ultrahigh Resolution Radiation Imaging System Using an Optical Fiber Structure Scintillator Plate." *Scientific Reports* 8, no. 1: 3194. https://doi.org/10.1038/s41598-018-21500-z.

Yamamoto, S., M. Yoshino, K. Kamada, et al. 2023. "Development of an Ultrahigh Resolution Real Time Alpha Particle Imaging System for Observing the Trajectories of Alpha Particles in a Scintillator." *Scientific Reports* 13, no. 1: 4955. https://doi.org/10.1038/s41598-023-31748-9.

Yamamoto, S., M. Yoshino, K. Nakanishi, K. Kamada, A. Yoshikawa, and J. Kataoka. 2024a. "Range and Light Output Measurements of Trajectory Images in a GAGG Plate With Different Alpha Particle Energies." *Journal of Instrumentation* 19, no. 1: P01010. https://doi.org/10.1088/1748-0221/19/01/P01010.

Yamamoto, S., M. Yoshino, K. Nakanishi, K. Kamada, A. Yoshikawa, and J. Kataoka. 2024b. "A Method for Estimating the Incident Directions of Alpha Particles in 2-Dimensional Trajectory Images in a GAGG Plate." *Journal of Instrumentation* 19, no. 4: T04010. https://doi.org/10.1088/1748-0221/19/04/T04010.

Zhu, Y., S. Qian, Z. Wang, et al. 2020. "Scintillation Properties of GAGG: Ce Ceramic and Single Crystal." *Optical Materials* 105: 109964. https://doi.org/10.1016/j.optmat.2020.109964.